IEEE Access
Multidisciplinary | Rapid Review | Open Access Journal

Received December 4, 2019, accepted December 30, 2019, date of publication January 7, 2020, date of current version January 17, 2020.

Digital Object Identifier 10.1109/ACCESS.2020.2964614

A Wearable Textile RFID Tag Based on an Eighth-Mode Substrate Integrated Waveguide Cavity

GIOVANNI A. CASULA[1], (Member, IEEE), GIORGIO MONTISCI[1], (Senior Member, IEEE), AND HENDRIK ROGIER[2], (Senior Member, IEEE)

[1]Dipartimento di Ingegneria Elettrica ed Elettronica, Università degli Studi di Cagliari, 09123 Cagliari, Italy
[2]IDLab-EM Group, imec-Ghent University, B-9052 Gent, Belgium

Corresponding author: Giorgio Montisci (giorgio.montisci@unica.it)

ABSTRACT A novel wearable textile Radio Frequency Identification (RFID) tag based on an eighth-mode substrate integrated waveguide cavity is presented. Antenna size reduction for effective operation in the [865-870]-MHz RFID UHF band is obtained by exploiting the H-field symmetry planes of a cylindrical Substrate Integrated Waveguide (SIW) cavity. High isolation from the human body and excellent robustness with respect to variations in antenna-body distance are achieved using an energy-based design strategy, aiming to reduce ground plane size. The resulting tag exhibits very low manufacturing complexity and may be produced at low-cost. Design and simulations were performed using CST Microwave Studio, and a prototype of the tag has been manufactured and tested in a real environment.

INDEX TERMS Eighth-mode substrate integrated waveguide (EMSIW), RFID, substrate integrated waveguide (SIW), textile antennas, wearable antennas.

I. INTRODUCTION

Mechanical robustness, easy manufacturing, low-cost, reduced size, light weight, flexibility, reliability in the proximity of the human body, and a low Specific Absorption Rate (SAR) are the main features that distinguish antennas for wearable devices from ''conventional'' antennas and that allow them to be efficiently integrated into a garment.

Though the most common applications of Radio Frequency Identification (RFID) technology are within logistics, retail, transportation, inventory management, manufacturing and security [3], [4], recently, interest is also growing for sensor networks [5]–[7], personal healthcare [8]–[10] and entertainment [11], [12]. Passive RFID tags are particularly suitable for these applications, since they do not require maintenance or regular recharging. Moreover, they usually have a long life and low production cost [3]. The tag device consists of a radio-frequency antenna with integrated microchip transponder, and, potentially, with additional appropriate sensors. In several applications, such as in body area networks or personal area networks, it must operate in proximity of, or attached to, the human body. In this regard, UHF wearable RFID systems are critical, since tag antennas must backscatter the power received from an interrogator while being deployed close to an extremely lossy platform, the human body. In addition, the tag antenna size must be kept as small as possible in the RFID frequency bands (from 865 to 970 MHz including European, US and Asia sub-bands), to ensure the comfort of the wearer, as required by on-body devices.

Several wearable RFID tag antennas have been proposed in recent literature [13]–[23]. Many of them have been designed using textile substrates, thus easing integration into clothes and garments [13], [16], [17], [22], [23]. These antennas exhibit low efficiency and gain due to the strong proximity of the human body. In addition, the robustness with respect to the distance from the human body [18], [20], [22] and the read range exhibit high variability, depending on the deployment conditions on the human body.

Recently, to increase the antenna-body isolation, wearable textile antennas based on Substrate Integrated Waveguide (SIW) cavities have been proposed in the 2.4 GHz ISM band and at higher frequencies [24]–[36]. These structures are particularly suitable for wearable applications since, in addition to the good isolation provided by the SIW technology, they ensure high flexibility [24], [26], [27], wideband/multiband operation [26], [27], a low-profile planar

The associate editor coordinating the review of this manuscript and approving it for publication was Mohammad Zia Ur Rahman.

structure and good radiation characteristics. Furthermore, antennas based on SIW cavities can be easily miniaturized by exploiting the symmetry of the field distributions of their resonant modes [24]–[36].

SIW antennas have widely demonstrated their potential for several applications at 2.4 GHz and beyond, using either coaxial cable or microstrip line feeding [24]–[47], leading to compact footprints. However, to the best of the authors' knowledge, up to now SIW technology has never been exploited for the design of a RFID passive wearable tag, especially in the lower part of UHF band (around 900 MHz), at which miniaturization remains a key challenge.

In this work, we propose a wearable textile RFID tag antenna based on an eighth-mode substrate integrated waveguide circular cavity (EMSIW), operating in the European UHF band (865-870 MHz). The EMSIW configuration minimizes the antenna size, while its ground plane is optimized, using the energy-based design strategy proposed in [37]–[41], to mitigate the deterioration in antenna performance due to the body coupling.

The Impinj Monza 4 integrated chip (IC) has been connected to the EMSIW cavity antenna. This microchip was appropriately positioned to minimize the perturbation of the electromagnetic field within the cavity, and to maximize the overall antenna efficiency.

A common closed-cell rubber foam is selected as a substrate, and adhesive copper coated non-woven PET fabric is employed for the metallization. The resulting tag antenna has a compact size ($8.73 \times 7.78 \times 0.4$ cm^3, which is $0.24 \times 0.22 \times 0.011\ \lambda_0^3$, with λ_0 the free-space wavelength at 868 MHz), yielding significantly smaller electrical dimensions compared to similar wearable SIW antennas described in the literature [24]–[36] (see Table 1 for a comparison), realizing a volume reduction by at least a factor of 7, and an area reduction by at least a factor of 2.5, in terms of free-space wavelength.

The antenna design and all the electromagnetic field simulations have been performed using CST Microwave Studio. Measurements have been performed in a real environment using a commercial RFID reader, showing high body-antenna isolation and good robustness with respect to variations of the antenna-body distance.

II. ANTENNA TOPOLOGY AND MATERIALS

The proposed SIW textile wearable antenna is designed for RFID Applications in the European UHF band, with a center frequency of 868 MHz. A 4 mm-thick closed-cell rubber foam, typically used in firefighter suits, has been selected as dielectric substrate for the SIW antenna. Its dielectric permittivity equals 1.3, with a loss tangent $tan\delta = 0.03$ (measured by means of the microstrip T-resonator method [48]). The metallization has been implemented using adhesive copper coated non-woven PET fabric, with a sheet resistivity of 0.04 Ω/square and a thickness of 0.11 mm. By following the formulas for SIW circular cavities specified in [49] as a starting point, we have designed a SIW cylindrical resonant cavity, operating in the TM_{010} mode at 868 MHz (Fig. 1a). The cavity diameter equals AB = 180 mm (Fig.1a). The radius of the vias is $R_H = 5$ mm, with a spacing $S_y = 16$ mm (Fig. 2). Next, we have taken advantage of the magnetic field symmetry of the TM_{010} mode to reduce the size of the cavity. First, a virtual magnetic wall has been placed along the horizontal symmetry plane of the SIW cavity, indicated by the line AOB in Fig. 1a. Then, the half of the cavity below the line AOB has been cut off, keeping a suitable ground plane extension G_e.

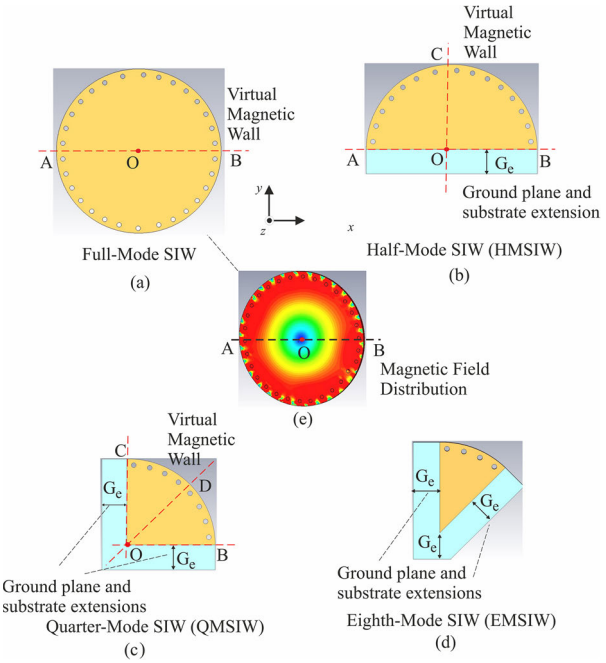

FIGURE 1. Design evolution: the symmetry of the first resonant mode is exploited to obtain the EMSIW structure. Full-Mode SIW (a); Half-Mode SIW (b); Quarter-Mode SIW (c); Eighth-Mode SIW (d); Electric field distribution of the TM_{010} mode for the Full-Mode circular SIW cavity as a function of applied field (e).

TABLE 1. Comparison between the wearable SIW proposed in the literature and our RIFD tag.

Ref.	Operating Frequency (GHz)	Antenna Size	Body effect	Feeding
[24]	2.45	$1.03 \times 1.07 \times 0.032\ \lambda_0^3$	Yes	Microstrip
[25]	4.45	$1.67 \times 1.25 \times 0.053\ \lambda_0^3$	No	Coax
[26]	2.45	$1.02 \times 0.76 \times 0.032\ \lambda_0^3$	Yes	Microstrip
[27]	2.45	$0.53 \times 0.44 \times 0.030\ \lambda_0^3$	Yes	Coax
[28]	5.20	$0.61 \times 0.69 \times 0.027\ \lambda_0^3$	No	Microstrip
[29]	2.45	$0.49 \times 0.49 \times 0.030\ \lambda_0^3$	Yes	Coax
[30]	2.45	$0.49 \times 0.33 \times 0.027\ \lambda_0^3$	No	Microstrip
[31]	2.45	$0.61 \times 0.39 \times 0.027\ \lambda_0^3$	Yes	Coax
[32]	5.8	$1.45 \times 0.81 \times 0.019\ \lambda_0^3$	Yes	Microstrip
[33]	5.8	$0.37 \times 0.37 \times 0.030\ \lambda_0^3$	Yes	Microstrip
[34]	5.8	$1.26 \times 0.77 \times 0.030\ \lambda_0^3$	Yes	CPW
[35]	5.8	$0.91 \times 0.80 \times 0.030\ \lambda_0^3$	Yes	Microstrip
[36]	2.45	$0.41 \times 0.41 \times 0.029\ \lambda_0^3$	Yes	Coax
This work	0.868	$0.24 \times 0.22 \times 0.011\ \lambda_0^3$	Yes	MicroCHIP

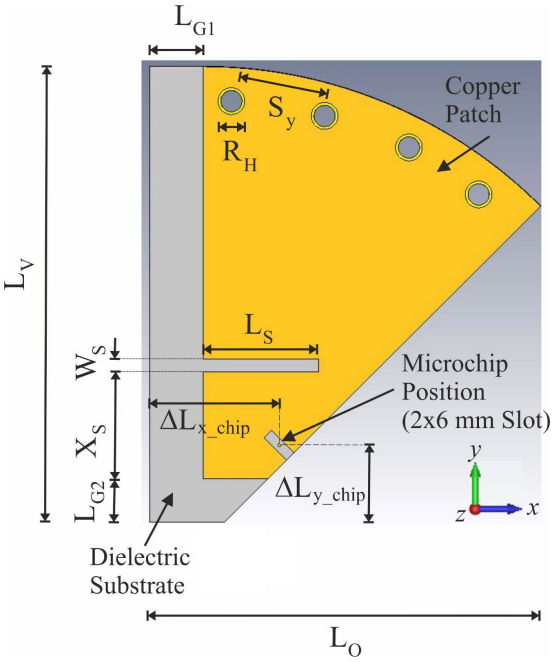

FIGURE 2. Layout of the designed SIW antenna.

In this way, a semi-circular cavity, resonating in half-mode SIW (HMSIW) operation, is obtained (Fig. 1b). Then, the same procedure has been applied to the semi-circular cavity, which has been halved by exploiting the vertical magnetic field symmetry plane indicated by the line CO in Fig. 1b. The result is the quarter-mode SIW resonator (QMSIW) shown in Fig. 1c. Finally, the latter has been further halved, cutting the QMSIW along the symmetry plane OD, to generate the eighth-mode SIW resonator (EMSIW) of Fig. 1d. The circular EMSIW operates as an effective broadside antenna, radiating an electric field through the open side walls with a maximum directed along the z-axis, propagating away from the wearer.

III. ANTENNA DESIGN AND SIMULATIONS

Following the design process described in Fig. 1, we obtain the antenna topology shown in Fig. 2, in which all the relevant geometrical parameters are clearly indicated.

The radiation characteristics of wearable antennas are strongly influenced by the proximity of the human body, which is a lossy and non-homogeneous material. Since the distance d between the body and the antenna changes randomly during actual operating conditions, it is important to maintain a stable performance regardless of the distance from the human body.

A numerical phantom has been added to the simulation scenario (Fig. 3), in order to investigate the effect of the body-antenna coupling. We have chosen a simplified phantom, consisting of a single layer with muscle-like dielectric properties at 868 MHz ($\varepsilon_r = 56.6$, $\sigma = 1.33$ S/m) and with a size of $250 \times 200 \times 100$ mm^3 [41].

The design has been performed using CST Microwave Studio with the antenna attached to the body phantom, being

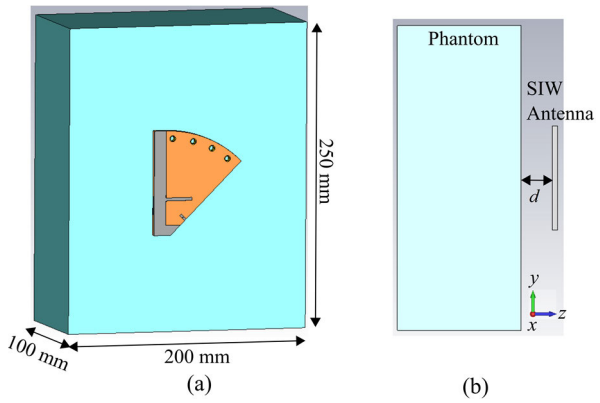

FIGURE 3. CST Microwave studio model of the designed antenna with the single layer body phantom: a) 3D view; b) side view.

for $d = 0$ (see Fig. 3). The main points of the design procedure, leading to the configuration of Fig. 2, are:

i) The addition of a slot of length L_S, cut out in the top patch. The slot lengthens the current path, further reducing the antenna size. Increasing L_S reduces the operating frequency, while the slot offset X_S can be used to fine tune the frequency. The slot width W_S is set to 2.5 mm. The optimized values at 868 MHz are $L_O = 77.8$ mm, $L_V = 87.3$ mm, $L_S = 21.7$ m, and $X_S = 19.9$ mm.

ii) The selection of a suitable feeding point for the connection of the microchip. The microchip has been placed along the diagonal side of the SIW cavity, as indicated in Fig. 2, since this location does not affect the electromagnetic field inside the cavity and allows easy matching of the antenna to the input impedance of the microchip (in our case a Impinj Monza 4 with an input impedance Z_{chip} equal to 13-j151 Ω at 868 MHz). Conjugate matching to Z_{chip} is achieved for $\Delta L_{x\_chip} = 24.3$ mm, $\Delta L_{y\_chip} = 14.4$ mm.

iii) The choice of the ground plane and dielectric substrate extensions G_e (Fig. 1d). Since the ground plane shields the antenna from the human body, a large ground plane improves the antenna robustness with respect to the human body proximity but increases the antenna dimensions. Therefore, an appropriate extension G_e of both the ground plane and the dielectric substrate should be kept in proximity of each virtual magnetic wall (see Fig. 1d) to achieve a trade-off between antenna robustness and its dimensions [37]–[41]. Table 2 reports the antenna input impedance Z_{in}, the power transmission coefficient $\tau = 4\ Re\ (Z_{chip})\ \mathrm{Re}\ (Z_{in})/|Z^*_{chip} + \mathrm{Z_{in}}|^2$, and its percentage variation with respect to $d = 0$ for three cases (see Fig. 4):

- *a)* No ground plane extension ($G_e = 0$ mm): $L_{G1} = L_{G2} = L_{G3} = 0$ (Fig. 4a);
- *b)* Ground plane extension of $G_e = 15$ mm along all the antenna sides: $L_{G1} = L_{G2} = L_{G3} = 15$ mm (Fig. 4b);

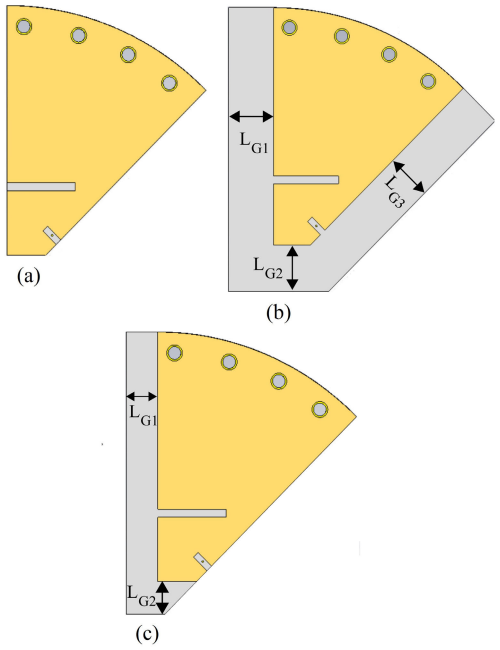

FIGURE 4. Different ground plane extensions for the proposed RDIF tag: a) No ground plane extension; b) Ground plane extension of Ge = 15 mm along all the antenna sides; c) Ground plane extension of Ge = 10 mm along the vertical side and no ground plane extension along the diagonal side.

TABLE 2. Comparison Between the RFID Tag Performance for different ground plane extensions.

case	d [mm]	Z_{in} [Ω]	τ	$\Delta\tau$ [%]
a)	**0**	**17 + j150**	**0.988**	**0**
	10	8.2 + j142.1	0.81	18.2
	20	7.2 + j141.2	0.73	26.1
	30	6.5 + j140.7	0.7	29.25
b)	**0**	**9.9 + j151.5**	**0.981**	**0**
	10	9.3 + j151.2	0.973	0.81
	20	8.5 + j151.1	0.96	2.1
	30	8.2 + j151.2	0.952	2.9
c)	**0**	**14.5 + j151**	**0.996**	**0**
	10	10.5 + j150.9	0.981	1.51
	20	9 + j150.6	0.96	3.61
	30	8.5 + j150.5	0.94	5.62

c) Ground plane extension of $G_e = 10$ mm along the vertical side and no ground plane extension along the diagonal side: $L_{G1} = L_{G2} = 10$ mm, $L_{G3} = 0$ (Fig. 4c).

From the results of Table 2, it appears that a reasonable trade-off between antenna dimensions and robustness is achieved in case *c*), resulting in the layout in Fig. 2, with $L_{G1} = 10$ mm and $L_{G2} = 10$ mm.

The design procedure described above is summarized in the flow diagram reported in Fig. 5.

The simulated frequency response of the designed antenna is shown in Fig. 6.

To assess the antenna robustness according to the energy-based design consideration of [37]–[41], in Fig. 7 the electric energy density distributions in the antenna substrate for $d = 0$ (antenna attached to the body) and $d = 30$ mm are reported at 868 MHz. The energy distributions are quite similar, confirming the low sensitivity of the designed antenna with respect to the human body proximity.

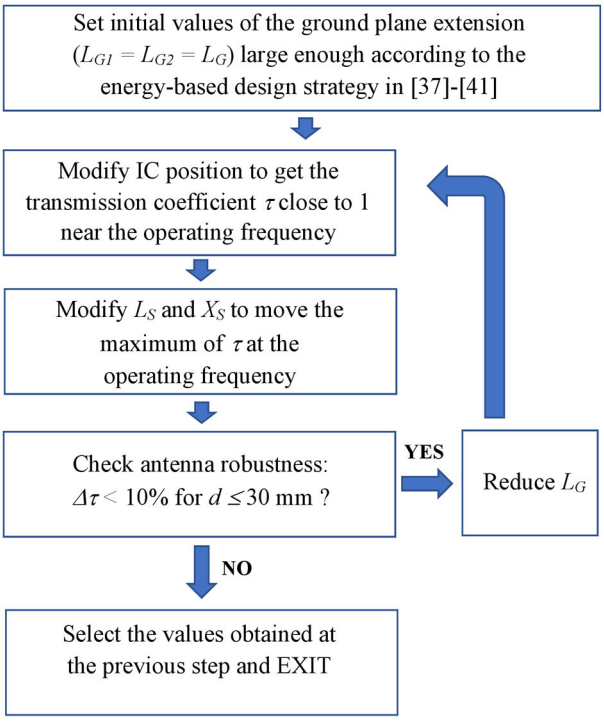

FIGURE 5. Flow diagram of the RFID tag design procedure.

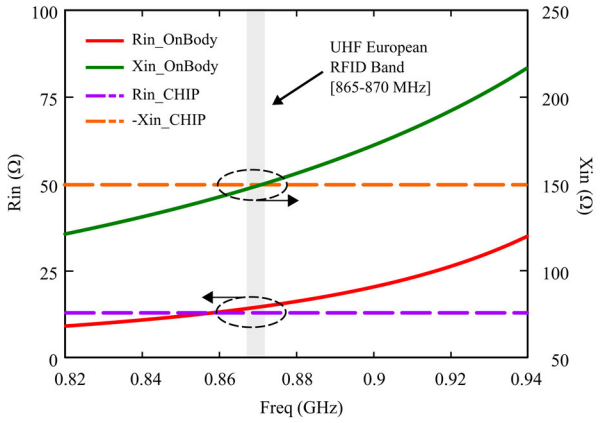

FIGURE 6. Simulated frequency response of the antenna in Fig. 2 for $d = 0$ (antenna attached to the body).

In Fig. 8, the simulated power transmission coefficient τ vs. frequency is shown for different spacings d between the antenna and the body phantom and, in Fig. 9, the variation of τ and the total efficiency $\tau \times \eta$ (η being the radiation efficiency), as a function of the antenna-body separation d, are reported at 868 MHz. From Figs. 8 and 9, is apparent that the transmission coefficient is quite stable with respect to different antenna-body separations. The antenna bandwidth is quite large: $\tau > 0.8$ in the range 850-890 MHz for $d = 0$, and in the range 859-885 MHz for $d = 30$ mm.

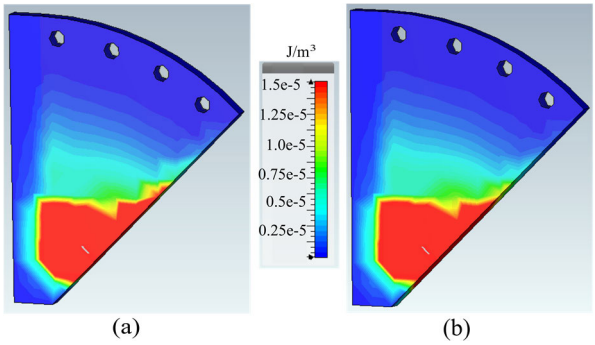

FIGURE 7. Simulated electric energy density distribution in the antenna substrate: RFID tag attached to the body ($d = 0$) (a); RFID tag at $d = 30$ mm from the body (b).

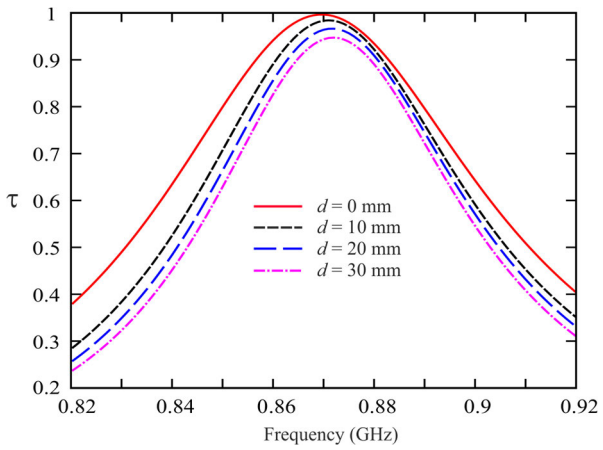

FIGURE 8. Simulated power transmission coefficient τ for different spacings of the antenna from the body phantom.

The total efficiency is about 16% for $d \in [0 - 30$ mm], which is a good value for a textile wearable RFID tag, due to the high dissipation in the body tissues and in the low-cost materials used to manufacture the tag (being the rubber foam and the textile conductive fiber). Wearable antennas with textile substrates available in the literature [13], [16], [17], [22], [23] provide lower values of efficiency (around 14% or less). However, a comparison with our configuration is not consistent since the efficiency strongly depends on the materials used. For this reason, we have focused on the ability of the proposed structure to provide high robustness and isolation with respect to human body coupling, which is a feature depending only on the proposed SIW architecture, and it is confirmed by the results reported in Figs. 8 and 9.

The CST Microwave Studio simulations confirm that the tag antenna's polarization is nearly linear along the y-axis when it is rotated by $\alpha = 20°$ in the xy-plane (see Fig. 10). The simulated surface current for $d = 0$ is also depicted in Fig. 10.

In Fig. 11, the normalized radiation pattern is reported for $\alpha = 20°$, for the antenna attached to the body ($d = 0$) and for a distance of $d = 30$ mm from the phantom, showing a cross-polarization in the broadside direction below -15 dB in both the principal planes.

Finally, table 3 reports the simulated Directivity and Gain in the broadside direction, at 868 MHz, of the SIW antenna

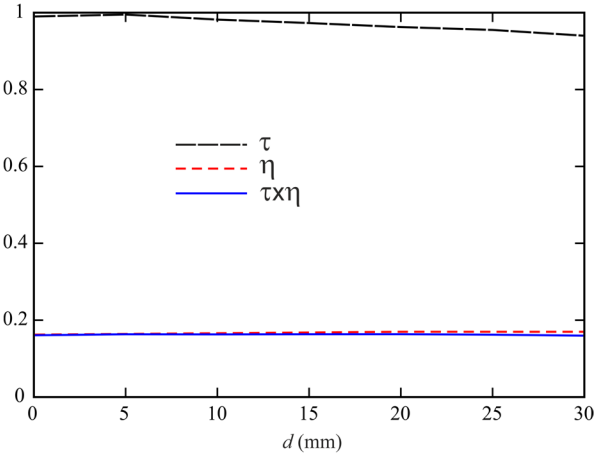

FIGURE 9. Simulated power transmission coefficient τ, radiation efficiency η and total efficiency $\tau \times \eta$, as a function of body-antenna separation d, at 868 MHz.

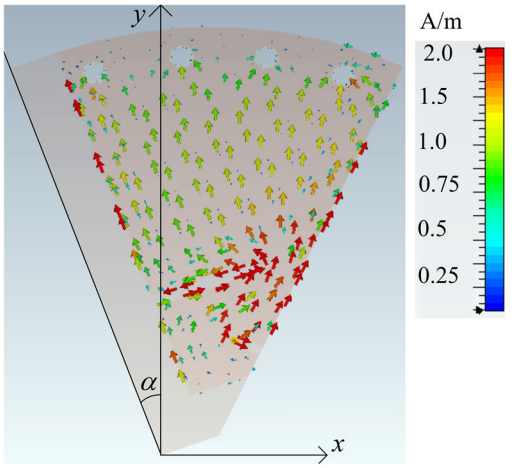

FIGURE 10. Surface current of the designed SIW antenna at 868 MHz for $d = 0$.

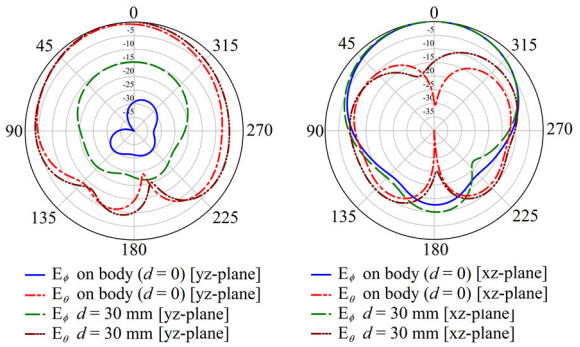

FIGURE 11. Simulated radiation pattern of the designed SIW antenna at 868 MHz for $\alpha = 20°$ (see Fig. 10).

fed by a discrete port instead of the microchip, for different body-antenna separations d.

IV. EXPERIMENTAL VERIFICATION

A prototype of the designed SIW RFID tag of Fig. 2 has been manufactured. The commercial chip Impinji Monza 4 has been connected to the antenna, soldering it to the patch at one

TABLE 3. Simulated directivity and gain of the SIW antenna at 868 MHz.

d [mm]	Directivity [dB]	Gain [dBi]
0	6.15	-2.60
10	5.70	-2.85
20	5.40	-3.05
30	5.65	-2.80

FIGURE 12. Prototype of the designed SIW antenna and measurement set up.

side, and to a via connected to the ground plane at the other side. The antenna prototype is depicted in Fig. 12.

To assess the robustness of this RFID tag, an artificial model of the human tissue has been synthesized. The human tissue has been experimentally simulated by using a simplified phantom, consisting of a PVC tank of dimension $25 \times 20 \times 10$ cm^3, having a thickness of 1 mm, filled with a tissue-simulating liquid with muscle-like parameters at 868 MHz ($\varepsilon_r = 56.6$, $\sigma = 1.33$ S/m), consisting of deionized water (53%), saccharose (45.6%) and sodium chloride (1.4%) [41].

The measurement setup has been deployed in a classroom at the University of Cagliari (Fig. 12). The floor of the premises is made of tiles over precast concrete and, therefore, we can assume as refractive index of the floor a value around 2.5 [3]. The ceiling is 3.5-meter high and the side walls are 4-meter far from the tag. In our case, their effect has been neglected.

A vertically polarized field incident on a horizontal floor will experience no reflection at the Brewster's Angle, which is around 68° in our case (measured w.r.t. the vertical). In this condition, reflection loss is above 15 dB for an incidence between 58° and 75°. For a reader antenna placed 0.8 m above the floor, the Brewster's angle reflection point is 2 m away, so the specularly reflected location is 4 m away.

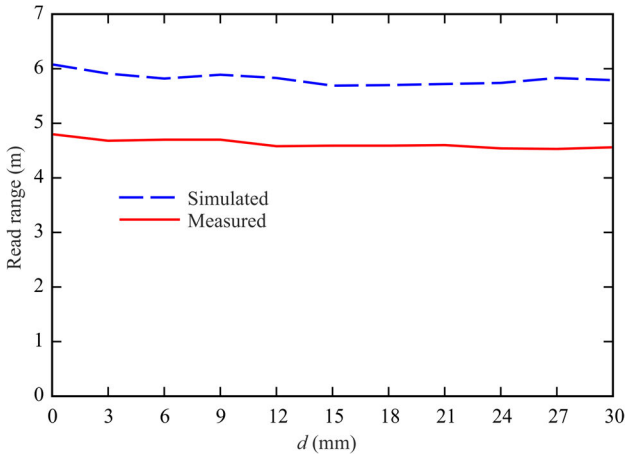

FIGURE 13. Simulated and measured read range of the RFID tag in Fig. 12.

The reflection point for incident angles of 58° and 75° is 1.3 m and 3 m away from the reader, respectively. Therefore, for RFID interrogator/tag separations between 2.6 m and 6 m the reflection loss remains above 15 dB. As we will see in the following, these values are within the measured read range of our RFID tag.

Based on the above considerations, the antenna is oriented in order to receive a nearly vertical polarization along the y-axis ($\alpha = 20°$ in Fig. 10), with the floor lying in the xz-plane. The tag is attached to the body phantom and placed in front of the commercial UHF reader Zebra RFD8500 Handheld [39], fixed on a mobile mount, and remote-controlled by a smartphone application via Bluetooth® wireless technology. The spacing between the antenna and the phantom has been modified by using pads of different thickness of expanded polystyrene (EPS), with dielectric permittivity close to 1.

The read range has been measured for different spacings between the antenna and the body phantom, and the results of the experimental verification, shown in Fig. 13, have been compared with the theoretical read range computed using the expression [50]:

$$r_{range} = \frac{\lambda}{4\pi}\sqrt{\frac{\frac{P_{CP}}{2} \cdot G_t \cdot G_{tag} \cdot \tau}{P_{chip}}} \tag{1}$$

The transmitter power is set to $P_{CP} = 30$ dBm (the reader antenna radiates circular polarization) and $G_t = 5.15$ dB, whereas the read sensitivity of the IC Monza 4 equals $P_{chip} = -17.4$ dBm. G_{tag} and τ have been computed using CST Microwave Studio.

The average measured read range is about 20% lower than the theoretical one (4.62 m vs. 5.82 m). This difference is probably due to the uncertainty in the estimation of the floor dielectric permittivity and to the path loss caused by the multipath fading generated by reflections on the ceiling and side walls. However, as expected, the read range remains stable when varying the antenna body-distance, which is the key feature of the proposed configuration, providing a validation of the simulated results in Figs. 8 and 9.

V. CONCLUSION

The SIW technology has been employed for the design of a wearable RFID tag operating in the European UHF band (865-870 MHz). Miniaturization is a key challenge at these frequencies. Then, exploiting the magnetic field symmetry of the TM_{010} mode of the circular SIW cavity, we have designed an Eighth-Mode SIW cavity antenna that allows to achieve a compact size of about 3900 $mm^2 \times 4$ mm. Moreover, thanks to the SIW architecture, the resulting RFID tag provides high isolation from the human body, and high robustness with respect to the antenna-body distance variation. Experimental assessment of the tag performance is obtained by measurement of the read range when the tag is housed in a classroom of our University.

REFERENCES

[1] P. S. Hall and Y. Hao, *Antennas and Propagation for Body-Centric Wireless Communications*. London, U.K.: Artech House, 2006.

[2] B. Latré, B. Braem, I. Moerman, C. Blondia, and P. Demeester, "A survey on wireless body area networks," *Wireless Netw*, vol. 17, no. 1, pp. 1–18, Jan. 2011.

[3] D. M. Dobkin, *The RF in RFID: UHF RFID in Practice*. New York, NY, USA: Elsevier, 2008.

[4] S. Tedjini, T. P. Vuong, V. Beroulle, and P. Marcel, "Radio-frequency identification systems from antenna characterization to system validation," in *Proc. Asia–Pacific Microw. Conf. (APCM)*, New Delhi, India, Dec. 2004.

[5] C. Douligeris and A. Mitrokotsa, "Integrated RFID and sensor networks: Architectures and applications," in *RFID and Sensor Networks: Architectures, Protocols, Security, and Integrations*. Boca Raton, FL, USA: Taylor & Francis, 2009, ch. 18, pp. 512–535.

[6] S. S. Anjum, R. M. Noor, M. H. Anisi, I. B. Ahmedy, F. Othman, M. Alam, and M. K. Khan, "Energy management in RFID-sensor networks: Taxonomy and challenges," *IEEE Internet Things J.*, vol. 6, no. 1, pp. 250–266, Feb. 2019.

[7] L. Wang, L. D. Xu, Z. Bi, and Y. Xu, "Data cleaning for RFID and WSN integration," *IEEE Trans. Ind. Informat.*, vol. 10, no. 1, pp. 408–418, Feb. 2014.

[8] K. Fan, S. Zhu, K. Zhang, H. Li, and Y. Yang, "A lightweight authentication scheme for cloud-based RFID healthcare systems," *IEEE Netw.*, vol. 33, no. 2, pp. 44–49, Mar. 2019.

[9] A. Sharif, J. Ouyang, Y. Yan, A. Raza, M. A. Imran, and Q. H. Abbasi, "Low-cost inkjet-printed RFID tag antenna design for remote healthcare applications," *IEEE J. Electromagn. RF Microw. Med. Biol.*, vol. 3, no. 4, pp. 261–268, Dec. 2019.

[10] G. A. Oguntala, R. A. Abd-Alhameed, N. T. Ali, Y.-F. Hu, J. M. Noras, N. N. Eya, I. Elfergani, and J. Rodriguez, "SmartWall: Novel RFID-enabled ambient human activity recognition using machine learning for unobtrusive health monitoring," *IEEE Access*, vol. 7, pp. 68022–68033, 2019.

[11] D. Czerwinski, M. Milosz, J. Montusiewicz, and M. Tokovarov, "The use of RFID technology to control a 3D model realising the gamification paradigm," in *Proc. IEEE Int. Conf. RFID Technol. Appl. (RFID-TA)*, Warsaw, Poland, Sep. 2017.

[12] T. Zhang, N. Becker, Y. Wang, Y. Zhou, and Y. Shi, "BitID: Easily add battery-free wireless sensors to everyday objects," in *Proc. IEEE Int. Conf. Smart Comput. (SMARTCOMP)*, Hong Kong, May 2017.

[13] T. Björninen, "Comparison of three body models of different complexities in modelling of equal-sized dipole and folded dipole wearable passive UHF RFID tags," *Appl. Comput. Electromagn. Soc. J.*, vol. 33, no. 6, pp. 706–709, Jun. 2018.

[14] G. M. Hatem, A. J. Salim, T. A. Elwi, H. T. Ziboon, J. H. Majeed, and J. K. Ali, "Wunderlich curve fractal dipole antenna for dual-band wearable RFID applications," *J. Eng. Appl. Sci.*, vol. 14, no. 4, pp. 1093–1099, Dec. 2019.

[15] S. Lopez-Soriano and J. Parron, "Wearable RFID tag antenna for healthcare applications," in *Proc. IEEE-APS Top. Conf. Antennas Propag. Wireless Commun. (APWC)*, Turin, Italy, Sep. 2015.

[16] B. Waris, L. Ukkonen, J. Virkki, and T. Björninen, "Wearable passive UHF RFID tag based on a split ring antenna," in *Proc. IEEE Radio Wireless Symp. (RWS)*, Jan. 2017, pp. 55–58.

[17] J. Virkki, Z. Wei, A. Liu, L. Ukkonen, and T. Björninen, "Wearable passive E-textile UHF RFID tag based on a slotted patch antenna with sewn ground and microchip interconnections," *Int. J. Antennas Propag.*, vol. 2017, Feb. 2017, Art. no. 3476017.

[18] T. Kaufmann, D. C. Ranasinghe, M. Zhou, and C. Fumeaux, "Wearable quarter-wave folded microstrip antenna for passive UHF RFID applications," *Int. J. Antennas Propag.*, vol. 2013, May 2013, Art. no. 129839.

[19] M. Akbari, L. Sydanheimo, Y. Rahmat-Sami, J. Virkki, and L. Ukkonen, "Implementation and performance evaluation of graphene-based passive UHF RFID textile tags," in *Proc. URSI Int. Symp. Electromagn. Theory (EMTS)*, Espoo, Finland, Aug. 2016.

[20] M.-C. Tsai, C.-W. Chiu, H.-C. Wang, and T.-F. Wu, "Inductively coupled loop antenna design for UHF RFID on-body applications," *Prog. Electromagn. Res.*, vol. 143, pp. 315–330, 2013.

[21] A. G. Santiago, J. R. Costa, and C. A. Fernandes, "Broadband UHF RFID passive tag antenna for near-body applications," *IEEE Antennas Wireless Propag. Lett.*, vol. 12, pp. 136–139, 2013.

[22] T. Kellomaki, "On-body performance of a wearable single-layer RFID tag," *IEEE Antennas Wireless Propag. Lett.*, vol. 11, pp. 73–76, 2012.

[23] S. Manzari, C. Occhiuzzi, and G. Marrocco, "Reading range of wearable textile RFID tags in real configurations," in *Proc. 5th Eur. Conf. Antennas Propag. (EUCAP)*, Rome, Italy, May 2011.

[24] R. Moro, S. Agneessens, M. Bozzi, and H. Rogier, "Wearable textile antenna in substrate integrated waveguide technology," *Electron. Lett.*, vol. 48, no. 16, pp. 985–987, Aug. 2012.

[25] T. Kaufmann and C. Fumeaux, "Wearable textile half-mode substrate-integrated cavity antenna using embroidered vias," *IEEE Antennas Wireless Propag. Lett.*, vol. 12, pp. 805–808, 2013.

[26] S. Lemey, F. Declercq, and H. Rogier, "Dual-band substrate integrated waveguide textile antenna with integrated solar harvester," *IEEE Antennas Wireless Propag. Lett.*, vol. 13, pp. 269–272, 2014.

[27] S. Agneessens and H. Rogier, "Compact half diamond dual-band textile HMSIW on-body antenna," *IEEE Trans. Antennas Propag.*, vol. 62, no. 5, pp. 2374–2381, May 2014.

[28] C. Jin, R. Li, A. Alphones, and X. Bao, "Quarter-mode substrate integrated waveguide and its application to antennas design," *IEEE Trans. Antennas Propag.*, vol. 61, no. 6, pp. 2921–2928, Jun. 2013.

[29] S. Agneessens, S. Lemey, T. Vervust, and H. Rogier, "Wearable, small, and robust: The circular quarter-mode textile antenna," *IEEE Antennas Wireless Propag. Lett.*, vol. 14, pp. 1482–1485, 2015.

[30] M. Mujumdar and A. Alphones, "Eighth-mode substrate integrated resonator antenna at 2.4 GHz," *IEEE Antennas Wireless Propag. Lett.*, vol. 15, pp. 853–856, 2016.

[31] M. E. Lajevardi and M. Kamyab, "Ultraminiaturized metamaterial-inspired SIW textile antenna for off-body applications," *IEEE Antennas Wireless Propag. Lett.*, vol. 16, pp. 3155–3158, 2017.

[32] Y. Hong, J. Tak, and J. Choi, "An all-textile SIW cavity-backed circular ring-slot antenna for WBAN applications," *IEEE Antennas Wireless Propag. Lett.*, vol. 15, pp. 1995–1999, 2016.

[33] D. Chaturvedi and S. Raghavan, "Compact QMSIW based antennas for WLAN/WBAN applications," *Prog. Electromagn. Res. C*, vol. 82, pp. 145–153, 2018.

[34] J. Lacik, T. Mikulasek, Z. Raida, and T. Urbanec, "Substrate integrated waveguide monopolar ring-slot antenna," *Microw. Opt. Technol. Lett.*, vol. 56, no. 8, pp. 1865–1869, Aug. 2014.

[35] D. Chaturvedi and S. Raghavan, "Circular quarter-mode SIW antenna for WBAN application," *IETE J. Res.*, vol. 64, no. 4, pp. 482–488, Jul. 2018.

[36] S. Agneessens, "Coupled eighth-mode substrate integrated waveguide antenna: Small and wideband with high-body antenna isolation," *IEEE Access*, vol. 6, pp. 1595–1602, 2018.

[37] G. A. Casula, A. Michel, P. Nepa, G. Montisci, and G. Mazzarella, "Robustness of wearable UHF-band PIFAs to human-body proximity," *IEEE Trans. Antennas Propag.*, vol. 64, no. 5, pp. 2050–2055, May 2016.

[38] A. Michel, R. Colella, G. A. Casula, P. Nepa, L. Catarinucci, G. Montisci, G. Mazzarella, and G. Manara, "Design considerations on the placement of a wearable UHF-RFID PIFA on a compact ground plane," *IEEE Trans. Antennas Propag.*, vol. 66, no. 6, pp. 3142–3147, Jun. 2018.

[39] G. A. Casula, G. Montisci, G. Valente, and G. Gatto, "A robust printed antenna for UHF wearable applications," *IEEE Trans. Antennas Propag.*, vol. 66, no. 8, pp. 4337–4342, Aug. 2018.

[40] G. Casula and G. Montisci, "A design rule to reduce the human body effect on wearable PIFA antennas," *Electronics*, vol. 8, no. 2, p. 244, Feb. 2019.
[41] G. A. Casula, A. Michel, G. Montisci, P. Nepa, and G. Valente, "Energy-based considerations for ungrounded wearable UHF antenna design," *IEEE Sensors J.*, vol. 17, no. 3, pp. 687–694, Feb. 2017.
[42] Y. Dong and T. Itoh, "Miniaturized substrate integrated waveguide slot antennas based on negative order resonance," *IEEE Trans. Antennas Propag.*, vol. 58, no. 12, pp. 3856–3864, Dec. 2010.
[43] A. P. Saghati, A. P. Saghati, and K. Entesari, "An ultra-miniature SIW cavity-backed slot antenna," *IEEE Antennas Wireless Propag. Lett.*, vol. 16, pp. 313–316, 2017.
[44] K. Kumar, S. Dwari, and M. K. Mandal, "Broadband dual circularly polarized substrate integrated waveguide antenna," *IEEE Antennas Wireless Propag. Lett.*, vol. 16, pp. 2971–2974, 2017.
[45] S. Mukherjee, A. Biswas, and K. V. Srivastava, "Broadband substrate integrated waveguide cavity-backed bow-tie slot antenna," *IEEE Antennas Wireless Propag. Lett.*, vol. 13, pp. 1152–1155, 2014.
[46] D.-Y. Kim, J. W. Lee, T. K. Lee, and C. S. Cho, "Design of SIW cavity-backed circular-polarized antennas using two different feeding transitions," *IEEE Trans. Antennas Propag.*, vol. 59, no. 4, pp. 1398–1403, Apr. 2011.
[47] C. Jin, Z. Shen, R. Li, and A. Alphones, "Compact circularly polarized antenna based on quarter-mode substrate integrated waveguide sub-array," *IEEE Trans. Antennas Propag.*, vol. 62, no. 2, pp. 963–967, Feb. 2014.
[48] K.-P. Latti, M. Kettunen, J.-P. Strom, and P. Silventoinen, "A review of microstrip t-resonator method in determining the dielectric properties of printed circuit board materials," *IEEE Trans. Instrum. Meas.*, vol. 56, no. 5, pp. 1845–1850, Oct. 2007.
[49] H. Dashti and M. H. Neshati, "Development of low-profile patch and semi-circular SIW cavity hybrid antennas," *IEEE Trans. Antennas Propag.*, vol. 62, no. 9, pp. 4481–4488, Sep. 2014.
[50] K. Rao, P. Nikitin, and S. Lam, "Antenna design for UHF RFID tags: A review and a practical application," *IEEE Trans. Antennas Propag.*, vol. 53, no. 12, pp. 3870–3876, Dec. 2005.

GIOVANNI A. CASULA (Member, IEEE) received the M.S. degree in electronic engineering and the Ph.D. degree in electronic engineering and computer science from the University of Cagliari, Cagliari, Italy, in 2000 and 2004, respectively.

Since December 2017, he has been an Associate Professor of electromagnetic fields at the University of Cagliari, teaching courses in electromagnetics and antenna engineering. He has authored or coauthored about 50 articles in international journals. His current research interests include the analysis and design of waveguide slot arrays, RFID Antennas, wearable antennas, and numerical methods in electromagnetics.

Dr. Casula is an Associate Editor of the *IET Microwaves, Antennas & Propagation*.

GIORGIO MONTISCI (Senior Member, IEEE) received the M.S. degree in electronic engineering and the Ph.D. degree in electronic engineering and computer science from the University of Cagliari, Cagliari, Italy, in 1997 and 2000, respectively.

Since November 2015, he has been an Associate Professor of electromagnetic fields at the University of Cagliari, teaching courses in electromagnetics and microwave engineering. He has authored or coauthored about 70 articles in international journals. His current research interests include the analysis and design of waveguide slot arrays, RFID Antennas, wearable antennas, numerical methods in electromagnetics, and microwave circuits and systems.

Dr. Montisci is an Associate Editor of IEEE Access, the *IET Microwaves, Antennas & Propagation*, and an Academic Editor of the *International Journal of Antennas and Propagation*.

HENDRIK ROGIER (Senior Member, IEEE) received the M.Sc. and Ph.D. degrees in electrical engineering from Ghent University, Ghent, Belgium, in 1994 and 1999, respectively.

From 2003 to 2004, he was a Visiting Scientist with the Mobile Communications Group, Vienna University of Technology, Vienna, Austria. He is a currently a Full Professor with the Department of Information Technology, Ghent University, a Guest Professor with the Interuniversity Microelectronics Centre, Ghent, and a Visiting Professor with the University of Buckingham, Buckingham, U.K. He has authored or coauthored over 160 articles in international journals and over 180 contributions in conference proceedings. His current research interests include antenna systems, radio wave propagation, body-centric communication, numerical electromagnetics, electromagnetic compatibility, and power/signal integrity. He is a member of the Technical Committee 24 on RFID Technology with the IEEE Microwave Theory and Techniques Society (MTT-S) and a member of the Governing Board of Topical Group MAGEO on Microwaves in Agriculture, Environment and Earth Observation with the European Microwave Association, Leuven, Belgium. He was a recipient of the URSI Young Scientist Award (twice) at the 2001 URSI Symposium on Electromagnetic Theory and at the 2002 URSI General Assembly, the 2014 Premium Award for Best Paper in the IET Electronics Letters, the Best Paper Award First Place in the 2016 IEEE MTT-S Topical Conference on Wireless Sensors and Sensor Networks, the Best Poster Paper Award at the 2012 IEEE Electrical Design of Advanced Packaging and Systems Symposium, the Best Paper Award at the 2013 IEEE Workshop on Signal and Power Integrity, and the Joseph Morrissey Memorial Award for the First Best Scientific Paper at BioEM 2013. He is an Associate Editor of the *IET Electronics Letters*, *IET Microwaves, Antennas and Propagation*, and the IEEE Transactions on Microwave Theory and Techniques. He acts as the URSI Commission B representative for Belgium.